DOI: http://dx.doi.org/10.15407/tpwj2018.11–12.10

ANODE PROCESSES IN WELDING ARCS

I.V. KRIVTSUN
E.O. Paton Electric Welding Institute of the NAS of Ukraine
11 Kazimir Malevich Str., 03150, Kyiv, Ukraine. E-mail: office@paton.kiev.ua

The paper describes the approaches to theoretical investigation and mathematical models of physical processes running in the anode layer of high-current (~ 10^2 A) electric arcs, burning in inert gas at atmospheric pressure. Numerical studies of anode processes in electric arcs with nonevaporating (water-cooled) anode, as well as in welding arcs (arcs with evaporating anode) were performed. It is shown that anode potential drop in the considered arcs is negative, having an essentially nonuniform distribution in the region of anode attachment of the arc. The latter circumstance largely determines the pattern of electric current flowing and energy transfer between arc plasma and anode (arc contraction on the anode or discharge distributed over anode surface). A procedure of calculation of effective anode drop in electric arcs is proposed, allowing for the above change of anode potential drop along the anode surface. 32 Ref., 1 Table, 15 Figures.

Keywords: *welding arc, arc plasma, arc column, anode layer, anode potential drop, heat flow into the anode, evaporation, mathematical modeling*

Fusion arc welding now is one of the main technological processes of producing permanent joints of metallic materials. Arc welding methods the most widely used in industrial production are consumable electrode welding in inert and active gases or in their mixtures (MIG/MAG), as well as inert-gas nonconsumable electrode welding (TIG), applied in fabrication of critical structures. Here we can also mention plasma welding as a variety of nonconsumable electrode welding, which allows an essential increase of penetration depth and thickness of metal being welded, respectively, due to application of a constricted arc. For effective application of electric arc as the welding heat source, it is necessary to have valid information about its thermal, electric and dynamic impact on the electrodes. In particular, at realization of the above welding methods, the anode processes have a quite important role, namely processes of interaction of arc plasma with electrode metal drop, which is the arc anode in the case of MIG/MAG welding, and with weld pool metal, which is the anode in the case of TIG and plasma welding. In the first case, the above processes determine wire melting, formation and transfer of electrode metal drops, and in the second case — penetration of the metal being welded and weld formation. As experimental determination of such important in terms of technology characteristics of the welding arc as electric current density and heat flow on the surface of the drop and the weld pool is difficult, because of high values of arc plasma temperature and molten metal surface temperature, smallness of geometrical dimensions of the arc attachment region and a number of other factors, theoretical study of anode processes, in particular by mathematical modeling, seems to be very relevant.

There are many approaches and models for numerical study of anode processes in free-burning and constricted (plasma) arcs (see, for instance, [1–8]). In the majority of them, however, arc plasma is assumed to be single-component, i.e. containing atoms and ions of shielding or plasma-forming, most often, inert gas. Plasma of the real welding arcs, is, as a rule, multicomponent, as, alongside the gas particles, it contains atoms and ions of evaporated material of the electrodes, primarily, of the anode [9]. Thus, the multicomponent nature of arc plasma should be taken into account at construction of an adequate mathematical model of anode processes in welding arcs.

Another important characteristic of such a model should be the possibility of allowing for the interconnection of physical processes running in the anode body, on its surface and in anode layer, with the processes in arc column. It should be noted that in the majority of works on complex modeling of electric, in particular, welding arc, quite simplified models of the anode region are used [10–15], whereas in the works devoted specifically to investigation of near-electrode phenomena (see, for instance, review [16] and literature cited there), processes running in the arc column, are given insufficient attention.

This study is devoted to description of self-consistent mathematical models and numerical study of physical processes, running in near-anode plasma of high-current (~ 10^2 A) electric arcs, burning in inert gas at atmospheric pressure, in particular welding arcs (allowing for anode material evaporation), for the conditions of MIG, TIG and plasma welding.

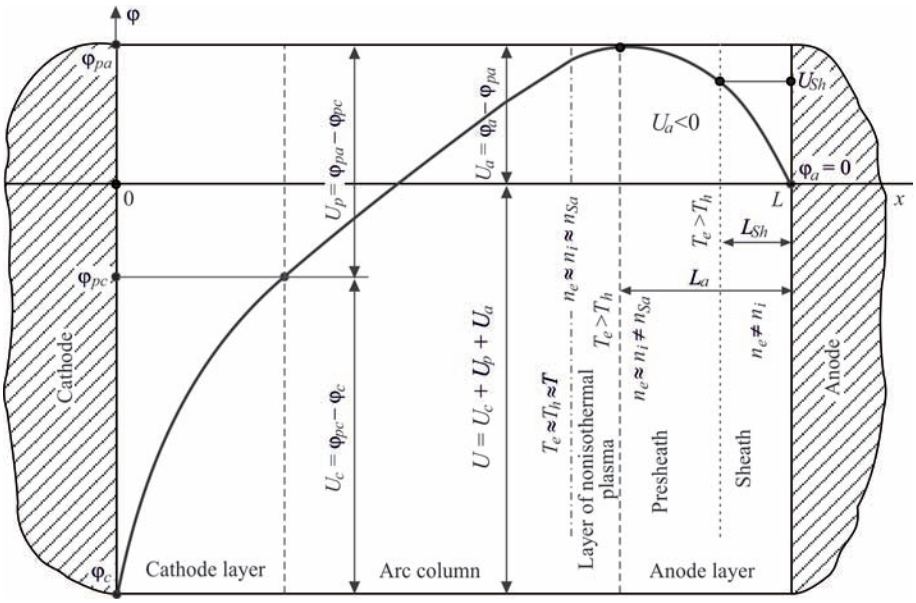

Figure 1. Distribution of electric potential along arc length: φ_c — cathode surface potential; φ_{pc} — potential of arc column plasma on the boundary with cathode layer; L — arc length (for other designations see the text)

Before beginning description of the above models, we will consider the characteristic distribution of electric potential by the length of atmospheric pressure high-current arc, which is shown in Figure 1. Electric arc can be conditionally divided into three regions: near-electrode layers of nonequilibrium plasma (cathode and anode) and arc column, where plasma is in the state of local thermodynamic equilibrium [17]. Here, total arc voltage U can be presented as a sum of voltage drops in cathode U_c and anode U_a layers, as well as in arc column U_p:

$$U = U_c + U_p + U_a. \quad (1)$$

Special attention should be given to the fact that in the considered arcs, in particular, welding arcs, anode potential drop, determined as $U_a = \varphi_a - \varphi_{pa}$, where φ_a is the potential of anode surface, φ_{pa} is the potential of arc column plasma on the boundary with the anode layer, is negative [2, 18–20]. Moreover, in view of the high conductivity of metallic materials, the anode surface is practically equipotential. Therefore, the anode electric potential φ_a can be considered constant with good approximation, and can be selected equal, for instance, to zero, as it was done in Figure 1. Then, considering the distributions of anode temperature along its surface and near-anode plasma characteristics, determining local values of anode drop, it can be stated that the potential of arc column plasma on the boundary with anode layer also is nonuniform in the region of arc anode attachment, i.e. it depends on the coordinate along the mentioned boundary [21]. This leads to appearance of the component of electric potential gradient and, accordingly, component of current density along the anode layer boundary, that largely determines the pattern of electric current flowing between arc plasma and anode. The noted facts are quite nontrivial and will be considered in detail in this work.

For description of arc plasma adjacent to anode surface, we will use the approach proposed in works [1–3], in terms of which the near-anode plasma can be conditionally divided into several zones, as shown in Figure 1 on the right. The first zone directly adjacent to the anode surface is a layer of space charge (Sheath), where the condition of plasma quasineutrality is disturbed and the part of potential drop between the plasma and anode is formed. This layer can be regarded as collisionless with sufficient accuracy, as at the pressure close to the atmospheric pressure, and plasma temperature values characteristic for the considered conditions $T \sim 1$ eV [1, 2], this layer thickness L_{Sh} commensurate with Debye radius $r_D \sim 10^{-8}$ m, is essentially smaller than the free path of near-anode plasma particles $l \sim 10^{-7}$–10^{-4} m (respective values of characteristic paths for atmospheric pressure Ar-plasma are given in Figure 2).

The second zone on the right in Figure 1 — the ionization layer or prelayer (Presheath), is the region of nonisothermal quasineutral multicomponent plasma, where the charged particles are generated due to plasma electrons ionizing the gas atoms, desorbing from the anode surface, and the evaporating atoms of anode material. The ions forming here are accelerated towards the anode surface by the electric field created by more mobile electrons, and recombine near this surface. Thus, the conditions of local ionization equilibrium are violated within the prelayer, i.e. concentrations of charged plasma particles $n_e \approx n_i$ differ from equilibrium concentration n_{Sa}, calculated

using Saha equations. In addition, a noticeable drop of near-anode plasma potential occurs here, which can be greater with its change in the space charge layer (see Figure 1).

The outer boundary of the anode layer runs at the distance from anode surface L_a, equal to several free paths of heavy plasma particles. The third zone starts behind this boundary, being the gas-dynamic region of arc plasma or the arc column, where local thermodynamic equilibrium is established. Note here that this region, in its turn, can be conditionally divided into two zones: layer of nonisothermal ionization-equilibrium plasma, the thickness of which is determined by value l_{ea} (see Figure 2), and within which equalizing of the temperature of electrons T_e and heavy particles T_h with plasma temperature in arc column T occurs, and the arc column proper (see Figure 1).

As under the considered conditions anode layer thickness $L_a \sim 10^{-4}$ m, as a rule, is by an order of magnitude smaller than the curvature radius of the surface of the anode (drop of electrode metal or weld pool) $R \sim 10^{-3}$ m, it can be considered almost flat at description of the processes, running in this layer. On the other hand, as L_a is much smaller than the characteristic scale of the change of parameters of arc plasma in gas-dynamic region, when considering the processes in arc column, the plasma anode layer can be regarded as infinitely thin. Thus, in terms of mathematical description of physical processes occurring in near-anode plasma of the welding arc, it can be divided into two regions: anode layer of nonequilibrium plasma, including the prelayer, as well as the layer of space charge, and arc column, for which the first region actually has the role of rupture surface.

Let us first consider the model of anode layer of a high-current arc, burning in inert gas at atmospheric pressure, provided that anode metal evaporation can be neglected. In this case, near-anode plasma can be considered one-component, containing atoms (a), single-charged ions (i) and electrons (e) of gas. We will neglect presence of multicharged ions in near-anode plasma that is a good enough approximation up to its temperature values of ~ 1.5 eV [22]. Moreover, we will assume that the heavy particles of plasma (atoms and ions) have common temperature T_h, which differs from electron temperature T_e (two-temperature model).

Following paper [23], we will use one-dimensional model of the anode layer. We will direct the x axis of the Cartesian coordinate system away from the anode into the plasma, and will regard the anode surface as flat and located at $x = 0$. Then, the basic equations of the model can be written as follows.

Continuity equations for electrons, ions and atoms of near-anode plasma:

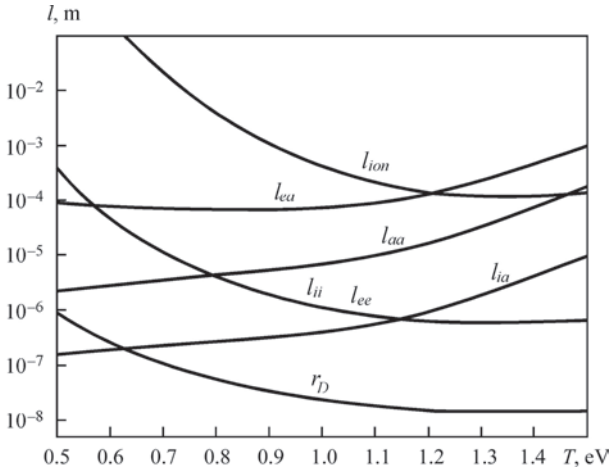

Figure 2. Characteristic lengths in equilibrium argon plasma at atmospheric pressure: r_D — Debye radius; l_{ee}, l_{ii}, l_{ia}, l_{aa}, l_{ea} — free paths relative to electron-electron, ion-ion, ion-atom, atom-atom and electron-atom collisions; l_{ion} — ionization length

$$\frac{dJ_\alpha}{dx} = \omega_\alpha, \quad \alpha = e, i, a. \tag{2}$$

Here $J_\alpha = n_\alpha \upsilon_\alpha$ is the flow density of particles of α species, where n_α and υ_α are the concentration and velocity of the respective particles; ω_α is the rate of change in the concentrations of plasma particles, owing to ionization-recombination reactions. As in atmospheric pressure discharges ionization occurs mainly through collision of electrons with atoms, and the dominating recombination mechanism is three-particle recombination involving an ion and two electrons, we can write

$$\omega_e = \omega_i = -\omega_a = k_i n_e n_a - k_r n_e^2 n_i, \tag{3}$$

where k_i, k_r are the constants of the processes of ionization and recombination, respectively. Adding up continuity equations for ions and atoms, and subtracting the respective equations for ions and electrons, we get

$$J_i = -J_a; \; J_i - J_e = j_a/e, \tag{4}$$

where j_a is the density of electric current in the anode layer; e is the elementary charge.

The first condition reflects the law of conservation of heavy particles of plasma, and the second — the continuity of electric current within the anode layer. It should be noted that relationships (4) can be used instead of any two continuity equations (2).

Equations of motion of plasma components can be written as [24]:

$$-\frac{dp_\alpha}{dx} + n_\alpha z_\alpha E + \sum_\beta \nu_{\alpha\beta}\mu_{\alpha\beta} n_\alpha n_\beta \left(\upsilon_\beta - \upsilon_\alpha\right) - \\ -R_\alpha^T = 0, \quad \alpha, \beta = e, i, a. \tag{5}$$

Here, $p_\alpha = n_\alpha k T_\alpha$ is the partial pressure of α-component of plasma, where k is the Boltzmann constant; T_α is the temperature of particles of α species; z_α is

the charge of the respective particles; E is the electric field intensity; $\upsilon_{a\beta}$, $\mu_{a\beta} = m_\alpha m_\beta/(m_\alpha + m_\beta)$ is the frequency of collisions with pulse transfer and reduced mass of particles of α and β species, where m_α is the mass of particles of α species; R_α^T is the thermodiffusion force, defined as follows

$$R_\alpha^T = C_\alpha^{(e)} n_\alpha k \frac{dT_e}{dx}, \quad (6)$$

where $C_\alpha^{(e)}$ is the coefficient of thermodiffusion of particles of α species. Note that the effect of thermodiffusion due to heavy particle temperature gradient is neglected.

Adding up equations (5) for all the components, we get the following relationship

$$-\frac{dp}{dx} + e\left(n_i - n_e\right)E = 0. \quad (7)$$

Here, $p = \sum_\alpha p_\alpha$ is the total pressure of plasma.

Equations of motion (5) should be complemented by Poisson equation for determination of electric field intensity

$$\varepsilon_0 \frac{dE}{dx} = e\left(n_i - n_e\right), \quad (8)$$

where ε_0 is the electric constant. Combining equations (7) and (8), we obtain the following relationship

$$\frac{d}{dx}\left(p - \varepsilon_0 E^2/2\right) = 0, \quad (9)$$

which means that total pressure in near-anode plasma, including pressure of electric field, is constant over the anode layer thickness.

Energy equations for electrons and heavy particles of plasma, neglecting convective transfer of energy by atoms and ions, have the following form:

$$\frac{d}{dx}\left(q_e + \frac{5}{2} J_e k T_e\right) = j_a E + \kappa_{eh} n_e k \left(T_h - T_e\right) - w_e; \quad (10)$$

$$\frac{dq_h}{dx} = \kappa_{eh} n_e k \left(T_e - T_h\right). \quad (11)$$

Here, q_e, q_h are the heat flows of electrons and heavy particles; k_{eh} is the frequency of energy exchange between the electrons and heavy particles; $w_e = U_i \omega_e - w_{rad}$ are the energy losses of electron component of plasma owing to nonelastic processes and radiation, where U_i is the ionization potential of gas atoms; w_{rad} are the radiation losses.

Ignoring the effect of thermodiffusion for atoms and ions, the heat flows of electrons and heavy particles of plasma can be represented in the following form:

$$q_e = -\lambda_e \frac{dT_e}{dx} + k T_e n_e \sum_\alpha A_\alpha^{(e)} \left(\upsilon_e - \upsilon_\alpha\right); \quad (12)$$

$$q_h = -\lambda_h \frac{dT_h}{dx}, \quad (13)$$

where λ_e, λ_h are the coefficients of heat conductivity of electrons and heavy particles, respectively; $A_\alpha^{(e)}$ is the kinetic coefficient.

Expressions given in [22, 23] can be used for calculation of the rates of ionization-recombination processes, transport and kinetic coefficients, as well as radiation energy losses, included into the equations of the described model.

Let us now go to the description of boundary conditions required for solving equations (2), (5), (8), (10), (11) in section $0 \le x \le L_a$. Edge conditions at $x = L_a$ (on the boundary of anode layer with arc column) are assigned proceeding from the taken assumption of the local thermodynamic equilibrium of plasma in arc column. Then, the concentrations of plasma particles on the above boundary can be determined from the equation of ionization equilibrium, law of partial pressures and condition of plasma quasineutrality:

$$k_i n_e n_a = k_r n_e^2 n_i; \quad (14)$$

$$p = n_e k T_e + n_i k T_h + n_a k T_h; \quad (15)$$

$$n_e = n_i. \quad (16)$$

At determination of temperatures T_h, T_e on the outer boundary of the anode layer, we will assume that plasma is isothermal here, i.e. we will include the layer of nonisothermal plasma (see Figure 1) into the anode layer, and will assume that Joule heating of plasma is balanced by radiation losses of electron energy. In this case at $x = L_a$ we can take

$$T_h = T_e; j_a E = w_{rad}(T_e). \quad (17)$$

Particle flows and electric field intensity on the outer boundary of the anode layer can be determined using relationships (4) and equations (5), allowing for the assumed uniformity of plasma in the arc column.

To assign edge conditions $x = 0$ (on anode surface) we will assume that all the charged particles, reaching this surface, are absorbed by it (partially recombine, and the remaining electrons form electric current in the anode body), and electron flow due to their emission from the anode material, is absent. Then, proceeding from kinetic considerations, the electron flow at $x = 0$ can be assigned as follows:

$$J_e = -\frac{n_e \bar{\upsilon}_e}{4}, \quad (18)$$

where $\bar{\upsilon}_e = \sqrt{8kT_e/\pi m_e}$ is the average velocity of thermal motion of electrons.

When assigning the edge condition for the ion flow to the anode surface, we will take into account the fact

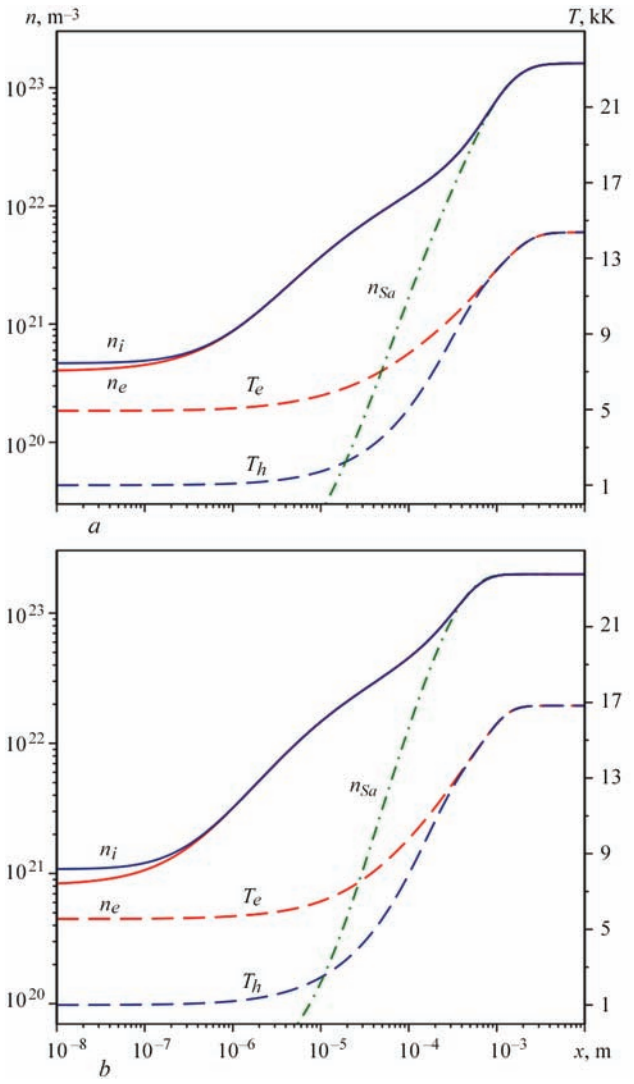

Figure 3. Distributions of the characteristics of atmospheric pressure argon arc plasma over the anode layer thickness for two values of anode current density: *a* — j_a = 700; *b* — 1500 A/cm^2. Solid curves show concentrations of electrons (n_e) and ions (n_i); dashed lines are temperatures of electrons (T_e) and heavy particles (T_h); dash-dotted line corresponds to charged particle concentration (n_{Sa}), calculated using Sakh equation

that the electron temperature near the above surface can be quite low $T \sim 0.5$ eV [22] and, according to Figure 2, the ion free path relative to collisions with atoms can turn out to be smaller than the Debye radius, i.e. thickness of the space charge layer. In this case, the space charge layer is collisional for ions, the flow of which at $x = 0$ can be defined through ion mobility in an electric field:

$$J_i = \frac{eEn_i}{\nu_{ia}\mu_{ia}n_a}. \qquad (19)$$

Electric field intensity near the anode surface, included into this expression, can be calculated by substituting expressions (18), (19) into the second condition (4) and using Poisson equations (8). In order to determine T_h, T_e at $x = 0$, we can use conditions from [23]:

$$T_h = T_s; \qquad (20)$$

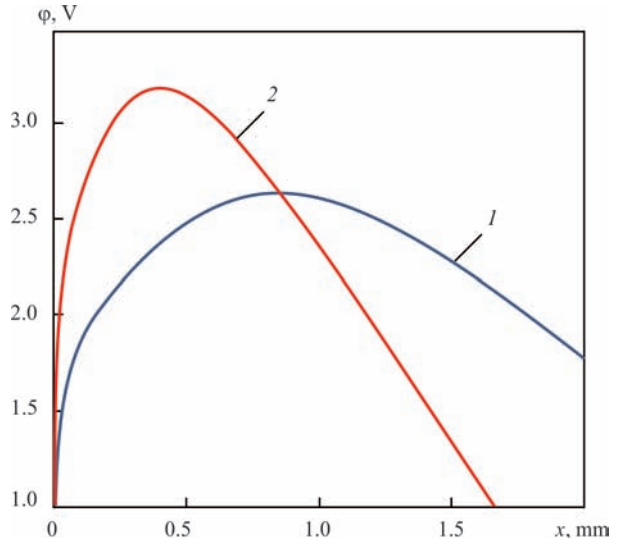

Figure 4. Distribution of electric potential over the thickness of argon arc anode layer at j_a, A/cm^2: *1* — 1000; *2* — 2000

$$-\frac{n_e\upsilon_e}{4}2kT_e = \frac{5}{2}J_ekT_e + q_e, \qquad (21)$$

where T_s is the anode surface temperature.

This completes description of the model of anode layer in an atmospheric pressure electric arc with non-evaporating anode. The model equations were solved numerically, and the solution algorithm is described in detail in [22]. Results of calculation of the characteristics of near-anode plasma of argon arc in a broad range of anode current densities j_a (5000–2000 A/cm^2) at pressure p = 1 atm and anode surface temperature T_s = 1000 K are given in Figures 3–6 and in the Table.

Figure 3, *a*, *b* shows the distributions of arc plasma characteristics over the anode layer thickness for two j_a values characteristic for high-current electric arcs, burning in argon at atmospheric pressure. As follows from calculated data given in these figures, the equilibrium plasma region (arc column), where $n_e \approx n_i \approx n_{Sa}$, $T_e \approx T_h$, is located at distance $x = L_a \leq$ $\leq$ 1 mm from anode surface. Here, the ionization region, where $n_e \approx n_i > n_{Sa}$, $T_e > T_h$, and the space charge layer, where $n_i > n_e$, are well resolved within the anode layer. Anode layer thickness L_a decreases at increase of anode current density that is related to increase of plasma temperature in arc column (from 13.53 kK at j_a = 500 A/cm^2 up to 18.04 kK at j_a = 2000 A/cm^2) and respective intensification of the processes of ionization and energy exchange between plasma components. As regards electron temperature near the anode surface, it weakly depends on anode current density, and at j_a changing from 500 to 2000 A/cm^2 it increases from 4.69 kK up to 5.99 kK.

Figure 4 presents the distribution of electric potential over the anode layer thickness. Here, the anode surface potential was assumed to be zero. As follows

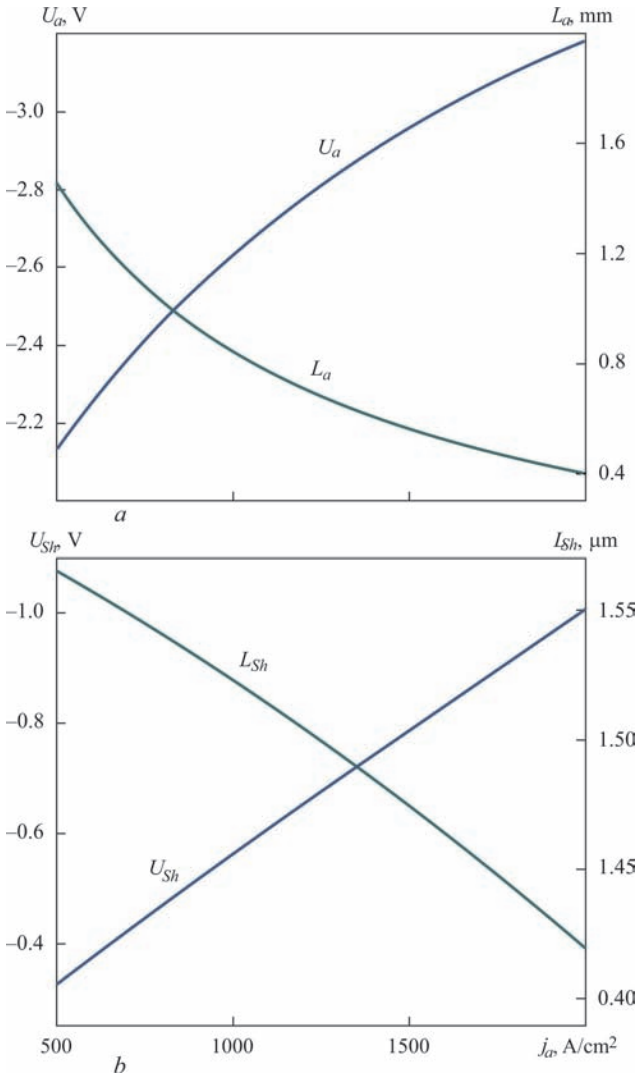

Figure 5. Anode layer thickness and anode potential drop (*a*); thickness of space charge layer and potential drop in this layer (*b*) for argon arc, depending on anode current density

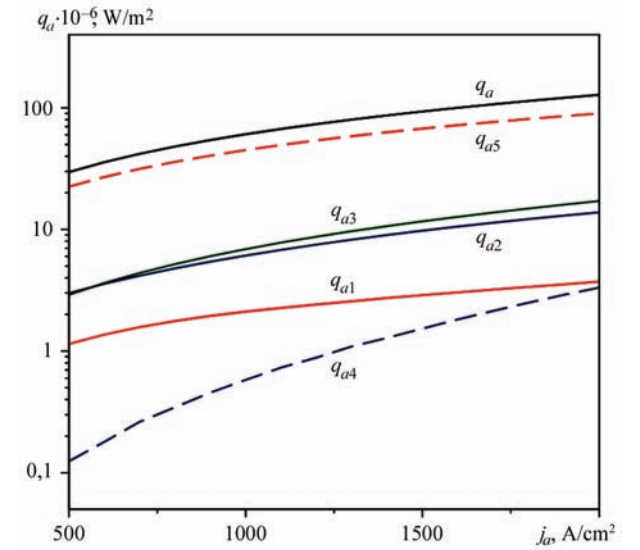

Figure 6. Total heat flow, applied to the anode by argon arc plasma, and its components, depending on anode current density

from calculated data, given in this figure, distribution of electric potential in near-anode plasma is essentially nonuniform and has a maximum. In the maximum point the electric field associated with charged particles concentration gradients is equal by absolute value, and is directed opposite to the electric field, causing conduction current in the plasma. Therefore, this is exactly the point that can be regarded as anode layer boundary $x = L_a$ and, according to earlier accepted definition, the value of anode drop U_a can be calculated as the difference of anode potential $\varphi_a = 0$ and potential value φ_{pa} on the above boundary (in maximum point). Dependencies of thus defined values L_a and U_a for atmospheric pressure argon arc with nonevaporating anode are given in Figure 5, *a*, from which it follows that anode layer thickness decreases with increase of anode current density, and anode drop increases by absolute value, remaining negative in the entire considered range of j_a, calculated U_a values being in good agreement with those measured experimentally [18].

Figure 5, *b* gives the dependence of thickness L_{Sh} of space charge layer defined as the distance between anode surface and point, in which the relative charge separation $\Delta_{Sh} = (n_i - n_e)/n_{es}$, where n_{es} — electron concentration at $x = 0$, is equal to 1 %, as well as dependence of potential drop U_{Sh} across the above layer on anode current density. Dependencies of L_{Sh} and U_{Sh} on j_a keep the tendencies inherent in the respective dependencies of L_a and U_a (see Figure 5, *a*, *b*) with the difference that the thickness of space charge layer changes only slightly with increase of current density.

Let us now consider the heat flow q_a contributed by arc plasma to the anode. The total heat flow can be represented as follows:

$$q_a = q_{a1} + q_{a2} + q_{a3} + q_{a4} + q_{a5}. \qquad (22)$$

Here, $q_{a1} = \lambda_e \frac{dT_e}{dx}$, $q_{a2} = \lambda_h \frac{dT_h}{dx}$ are the heat flows due to heat conductivity of electrons and heavy particles, respectively; $q_{a3} = -\frac{5}{2} J_e kT_e - kT_e n_e \sum_{\alpha=i,a} A_\alpha^{(e)} \left(\upsilon_e - \upsilon_\alpha\right)$ is the heat flow due to convective energy transfer by plasma electrons; $q_{a4} = -J_i U_i$, $q_{a5} = (J_i - J_e)\varsigma_a$ (where ς_a is the work function of anode material) are the components of heat flow to the anode, due to recombination of ions and absorption of electrons by its surface.

Dependencies of heat flow q_a and its components on j_a at $\varsigma_a = 4.5$ eV that corresponds to steel anode, are given in Figure 6. As follows from the presented dependencies, electron absorption by anode material makes the main contribution to the heat flow, and the next most important components are convective transfer of electron energy and the heat flow due to

heat conductivity of heavy particles. As regards calculated values of q_a and its components, they are in good agreement with the results of calculations performed in [6], and results of measurements taken by the authors of [18].

Completing description of the results of modeling the characteristics of near-anode plasma of atmospheric pressure argon arc with nonevaporating anode, we present a summary table of calculated values of anode layer thickness L_a, anode potential drop U_a, heat flow to the anode q_a and volt equivalent of heat on the anode $V_a = q_a/j_a$ for atmospheric pressure argon arc at different values of anode current density j_a.

Let us now consider a simplified model of physical processes in near-anode plasma of the welding arc for the conditions of MIG, TIG or plasma welding. Under the thermal impact of the arc on electrode metal or metal being welded (anode), the surface of the drop or weld pool can be locally heated up to temperatures, comparable with metal boiling temperature T_B. As a result of anode metal evaporation, welding arc plasma, as was already mentioned, becomes multicomponent, containing, alongside the particles of shielding or plasma-forming gas also the atoms and ions of metal vapour.

At analysis of physical processes running in anode layer of multicomponent plasma of the welding arc, we will assume that on the outer boundary of this layer arc plasma is characterized by the following parameters: n_e^0 — electron concentration; $n_{\alpha Z}^0$ — concentration of atoms ($Z = 0$) and ions ($Z = 1$) of shielding or plasma-forming gas. ($\alpha = g$), atoms ($Z = 0$) and ions ($Z = 1, 2$) of metal vapour ($\alpha = m$); Ze – ion charge; T_e^0 — electron temperature; T_h^0 — temperature of heavy plasma particles, assumed to be the same for all atom and ion species, but different from T^0_e (two-temperature plasma model); m_e — electron mass; M_α — masses of heavy particles (atoms and ions) of shielding gas ($\alpha = g$) and metal being welded or electrode metal ($\alpha = m$). As was already noted, the anode layer of welding arc plasma can be regarded as flat, that is why we will consider the values of concentrations n_e^0, $n_{\alpha Z}^0$, temperatures T_e^0, T_h^0 and normal to anode surface component of current density $j_a \equiv j_{an}$ in the region of anode attachment of the arc, as local values, corresponding to a given point of anode surface and characterized by certain value of temperature T_s.

We will, as we did earlier, assume that electric current transfer between arc plasma and anode is carried only by electrons and ions, coming from plasma (all the ions trapped on the anode surface, recombine there, and come back in the form of atoms, while the flow of electrons emitted by its surface, is negligibly small). Then, the total density of electric current between arc plasma and anode can be represented as

$$j_a = j_e - j_i, \quad (j_a > 0). \tag{23}$$

Here j_e is the density of current of plasma electrons, reaching the anode surface; $j_i = \sum\limits_{\alpha=m,g;\, Z\geq 1} j_{\alpha Z}$ is the total density of ion current to anode surface (for ions of all species and charges).

Following [25] further we will approximate the electron component of arc plasma within the anode layer as collisionless (see Figure 2), and electron temperature as constant over its thickness. Moreover, as plasma potential on the anode layer boundary φ_{pa} is higher than anode surface potential φ_a [2, 18–20], electrons are decelerated by the electric field, while ions are accelerated towards this surface. In this case, electron current density between the plasma and anode can be written as [2, 3]:

$$j_e = \frac{1}{4} e n_e^0 \bar{\upsilon}_e^0 \exp\left(-\frac{e\varphi_{pa}}{kT_e^0}\right), \tag{24}$$

where $\bar{\upsilon}_e^0 = \sqrt{8kT_e^0/\pi m_e}$ is the thermal velocity of electrons on the anode layer outer boundary.

Here, it should recalled that owing to high conductivity of anode metal, compared to that of near-anode plasma, its surface potential is practically constant in the region of anode attachment of the arc and is assumed to be zero (see Figure 1).

In order to determine ion currents, it is necessary to consider the processes in the ionization region, where ion generation and their acceleration towards the anode surface occur. For this purpose, we use an approach [26], which is based on the assumption that ion free path relative to Coulomb intercollisions l_{ii} is much smaller than ionization length l_{ion} and their free path relative to collisions with atoms l_{ia} (see Figure 2). This suggests that all the ions in the prelayer are intensively maxwellized and acquire a common velocity of directional movement, the value of which on the boundary of ionization region with space charge layer in the diffusion mode of anode metal evaporation is determined by the following expression [25]:

Main characteristics of the arc anode layer, depending on anode current density

$j_a \cdot 10^{-4}$, A/m^2	$L_a \cdot 10^{-3}$, m	U_a, V	$q_a \cdot 10^{-6}$, W/m^2	V_a, V
500	1.46	– 2.13	21.5	4.30
700	1.14	– 2.36	30.3	4.33
1000	0.84	– 2.63	43.9	4.39
1500	0.56	– 2.96	67.6	4.51
2000	0.40	– 3.18	92.7	4.64

$$V_{i_{Sh}} \equiv V_i(L_{Sh}) = \sqrt{\frac{\sum\limits_{\alpha=m,g;\, Z\geq 1} k\left(ZT_e^0 + T_h^0\right)n_{\alpha Z}^0}{\sum\limits_{\alpha=m,g;\, Z\geq 1} m_\alpha n_{\alpha Z}^0}}. \qquad (25)$$

Selecting as the boundary of the prelayer with space charge layer such an $x = L_{Sh}$, at which the condition of plasma quasineutrality is disturbed [27], we find the concentrations of charged particles on this boundary [25]:

$$n_{e_{Sh}} \equiv n_e(L_{Sh}) = n_e^0 \exp\left(-\frac{1}{2}\right);$$
$$n_{\alpha Z_{Sh}} \equiv n_{\alpha Z}(L_{Sh}) = n_{\alpha Z}^0 \exp\left(-\frac{1}{2}\right), \qquad (26)$$
$$\alpha = m, g; \quad Z \geq 1.$$

The ion currents to anode surface can be written as follows:

$$j_{\alpha Z} = Zen_{\alpha Z}^0 \exp\left(-\frac{1}{2}\right)V_{i_{Sh}}, \quad \alpha = m, g; Z \geq 1. \qquad (27)$$

Knowing the electron and ion currents to anode surface, it is easy to find from equation (23) the plasma potential φ_{pa} relative to the specified surface

$$\varphi_{pa} = \frac{kT_e^0}{e}\ln\left(\frac{en_e^0\bar{\upsilon}_e^0}{4\left[j_a + \sum\limits_{\alpha=m,g;\, Z\geq 1} j_{\alpha Z}\right]}\right). \qquad (28)$$

The anode potential drop U_a is more often used in welding publications instead of φ_{pa} value. It is defined as the difference of potentials between anode surface and outer boundary of anode layer of arc plasma. Considering that anode surface potential was taken to be zero at φ_{pa} definition, we obtain $U_a = -\varphi_{pa}$. Thus, as was already noted, the anode potential drop is negative in welding arcs. Moreover, taking into account the respective distributions of values, included into expression (28), along the anode surface φ_{pa} can be essentially nonuniform in the region of anode attachment of the arc, i.e. it can depend on the coordinate along anode layer boundary. This may lead to appearance of the component of electric potential gradient, and, accordingly, component of current density along the boundary of arc column with anode layer, the direction and magnitude of which determine the pattern of electric current flowing between the arc plasma and the anode (arc contraction on the anode or discharge distributed over the anode surface).

Calculation of the distributions of j_e, $j_{\alpha z}$, φ_{pa} or U_a values along the boundary of anode layer with arc column requires knowledge of the respective distributions of temperatures T_e^0, T_h^0 and concentrations n_e^0, $n_{\alpha Z}^0$ of charged particles on the mentioned boundary, as well as distributions of normal to the anode surface component of electric current density j_a. Assuming the multicomponent plasma in welding arc column to be ionization-equilibrium, the composition of such plasma in each point of the mentioned boundary can be determined using the following system of equations:

Sakh equations allowing for plasma nonideality

$$\frac{n_e^0 n_{\alpha Z+1}^0}{n_{\alpha Z}^0} = \left(\frac{2\pi m_e kT_e^0}{h^2}\right)^{3/2}\frac{2\theta_{\alpha Z+1}}{\theta_{\alpha Z}}\times$$
$$\times\exp\left[-\frac{e\left(U_{\alpha Z} - \Delta U_Z\right)}{kT_e^0}\right], \quad \alpha = m,\ g;\ Z \geq 0. \qquad (29)$$

Here h is the Planck's constant; $\theta_{\alpha Z}$ are the statistical sums for heavy particles of α species, which are in charge state Z; $U_{\alpha Z}$ are the ionization potentials (for transition of particles of α species from charge state Z into $Z + 1$); $\Delta U_Z = (e(Z + 1))/r_D$ are the reductions of ionization potentials, which are due to interaction of charged particles in the plasma [28], where

$$r_D = \left[kT_e^0\varepsilon_0 \Big/ e^2\left(n_e^0 + \frac{T_e^0}{T_h^0}\sum_{\alpha=m,g;\, Z\geq 1} n_{\alpha Z}^0 Z^2\right)\right]^{1/2}$$

is the Debye radius.

Condition of multicomponent plasma quasineutrality

$$n_e^0 = \sum_{\alpha=m,g;\, Z\geq 1} n_{\alpha Z}^0 Z. \qquad (30)$$

Law of partial pressures

$$p = n_e^0 kT_e^0 + \sum_{Z\geq 0} n_{mZ}^0 kT_h^0 + \sum_{Z\geq 0} n_{gZ}^0 kT_h^0 - \Delta p. \qquad (31)$$

Here, p is the plasma pressure near the anode surface; $\Delta p = \frac{1}{6}\frac{e^2}{r_D}\left(n_e^0 + \sum\limits_{\alpha=m,g;\, Z\geq 0} n_{\alpha Z}^0 Z^2\right)$ is the pressure lowering, because of plasma nonideality [28].

In order to close the system of equations (29)–(31), one more condition is required, which determines the distribution of the concentration of heavy particles (atoms and ions) of metal vapour along the anode layer boundary. In the diffusion mode of anode metal evaporation, assuming that the rate of vapour diffusion in arc plasma is small, i.e. vapour state is close to saturation, we can select as such a condition the equality of local value of partial pressure of evaporated metal heavy particles on the above boundary to the saturated vapour pressure p_s over the metal surface, having the respective temperature value T_s:

$$\sum_{Z\geq 0} n_{mZ}^0 kT_h^0 = p_s \equiv p_0 \exp\left[\frac{\lambda_v}{k}\left(\frac{1}{T_B} - \frac{1}{T_s}\right)\right], \qquad (32)$$

where p_0 is the atmospheric pressure; λ_v is the work function of anode metal atom; $T_h^0 = T_s$.

As an example, Figure 7 gives the thus calculated values of anode potential drop U_a as a function of T_e^0, j_a and T_s under the conditions, characteristic for TIG welding of low-carbon steel (Fe is the evaporating element) in argon. As follows from calculated data presented in this figure, the values of anode potential drop are negative, increasing by absolute value with increase of electron temperature of plasma near the anode, as well as its surface temperature (see Figure 7, *a*, *c*), and somewhat decreasing with j_a increase (see Figure 7, *b*). Value U_a for the considered conditions falls in the range from –1 to –4 V, that correlates quite well with the experimental data of [18], and in the case of small values of anode surface temperature, when evaporation of its material can be neglected, with the results of calculations made in [22] for non-evaporating anode.

Let us now consider the processes of energy transfer in anode layer of multicomponent plasma of the welding arc. Heat flow q_a from near-anode plasma to the surface of metal being welded can be represented as follows:

$$q_a = q_e + q_i, \tag{33}$$

where q_e, q_i are the flows of potential and kinetic energy, carried by plasma electrons and ions, respectively.

Expression for q_e can be written in a simplified form as [2, 18]:

$$q_e = j_e\left(\frac{5kT_e^0}{2e} + \zeta_a\right). \tag{34}$$

Considering the initial energy of ions on the outer boundary of space charge layer, as well as their additional acceleration in this layer, we can write for q_i

$$q_i = \sum_{\alpha=m,g;\, Z\geq 1} j_{\alpha Z}\left(\varphi_{Sh} + \frac{M_\alpha V_{i_{Sh}}^2}{2Ze} + \frac{1}{Z}\sum_{Z'=1}^{Z} U_{\alpha Z'} - \zeta_a\right), \tag{35}$$

where $\varphi_{Sh} \equiv \varphi(L_{Sh}) = \varphi_{pa} - \frac{1}{2}\frac{kT_e^0}{e}$ is the potential of arc plasma on the boundary of space charge layer (see Figure 1).

Expression (33) can be rewritten as

$$q_a = j_a V_a, \tag{36}$$

where V_a is the value of volt equivalent heat, released on the anode, which, unlike the respective value of anode drop U_a, is always positive (see Table). Considering (33)–(35) for calculating V_a we find

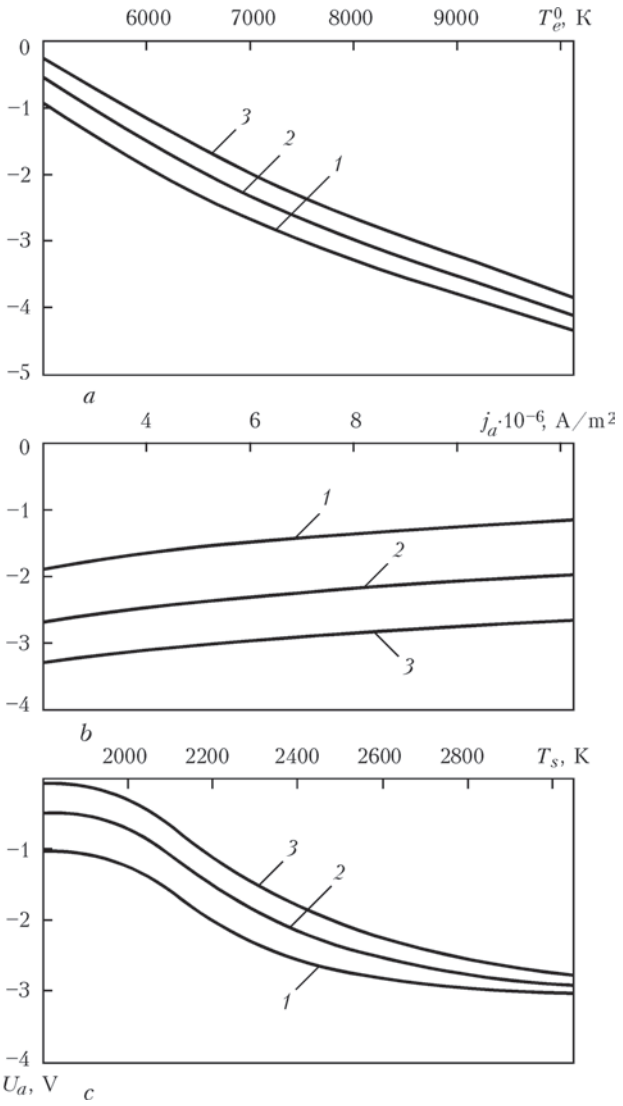

Figure 7. Dependencies of anode potential drop on electron temperature on anode layer boundary (*a*), anode current density (*b*) and its surface temperature (*c*) under the conditions, characteristic for TIG welding of low-carbon steel in argon: *a* — T_s = 2472 K (*1* — $j_a = 2\cdot10^6$; *2* — $5\cdot10^6$; *3* — 10^7 A/m²); *b* — T_s = 2472 K (*1* — $T_e^0 = 6\cdot10^3$; *2* — $7\cdot10^3$; *3* — $8\cdot10^3$ K); *c* — $T_e^0 = 7\cdot10^3$ K (*1* — $j_a = 2\cdot10^6$; *2* — $5\cdot10^6$; *3* — 10^7 A/m²)

$$V_a = \zeta_a + \frac{j_e}{j_a}\frac{5kT_e^0}{2e} + \sum_{\alpha=m,g;\, Z\geq 1} \frac{j_{\alpha Z}}{j_a}\left(\varphi_{Sh} + \frac{M_\alpha V_{i_{Sh}}^2}{2Ze} + \frac{1}{Z}\sum_{Z'=1}^{Z} U_{\alpha Z'}\right). \tag{37}$$

Figure 8 shows the results of calculations of the heat flow to the anode as a function of T_e^0, j_a and T_s under the conditions, characteristic for TIG welding of low-carbon steel in argon. As follows from the given calculated dependencies, value q_a increases with electron temperature in plasma anode layer, normal component of anode current density and its surface temperature, this tendency being the strongest in $q_a(T_s)$ dependence (see Figure 8, *c*).

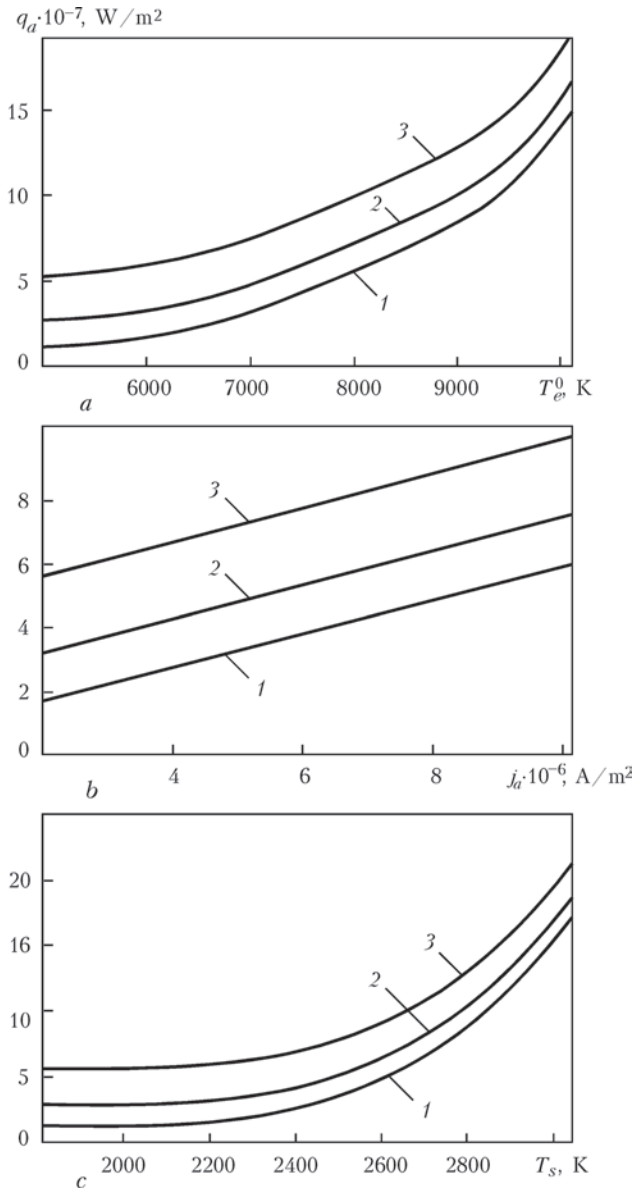

Figure 8. Dependencies of heat flow to the anode on electron temperature on anode layer boundary (*a*), anode current density (*b*) and its surface temperature (*c*) under the conditions characteristic for TIG welding of low-carbon steel in argon (parameters and designations are the same as in Figure 7)

Let us now consider the distributions of near-anode plasma characteristics along the boundary of anode layer with welding arc column for the conditions of TIG welding of low-carbon steel in argon atmosphere. For calculation of the temperature and composition of multicomponent plasma on the mentioned boundary, determining the respective distributions of values φ_{pa} or U_a, j_a and q_a over the region of anode attachment of the arc, we will use the proposed in [29] and modified in [30] self-consistent model of the processes of energy-, mass- and charge-transfer in the column and anode region of an electric arc, burning between a refractory cathode and flat evaporating anode.

We will consider two characteristic variants of thermal state of the anode, namely diffusively evaporating anode (Fe is the evaporating element) and water-cooled (nonevaporating) anode with surface temperature T_s = 500 K. In the first case, we assume that the anode surface temperature in the region of the arc anode attachment changes by an exponential law $T_s(r) = (T_{s0} - T_\infty)\exp(-a^2r^2) + T_\infty$ and in the center of this region it reaches value T_{s0}, not exceeding the temperature, at which evaporation goes into the convective mode [25]. Here, r is the radial coordinate, calculated from the arc axis; T_∞ = 500 K is the surface temperature at considerable distance from the axis, and concentration rate a is defined so that the radius of molten zone on steel anode surface was equal to 2.5 mm [21].

Calculations of spatial distributions of temperature, composition and other characteristics of near-anode arc plasma were conducted at the following parameters: arc length L = 3 mm; arc current I = 200 A; anode surface temperature T_{s0} in the center of arc attachment region was varied in the range from 500 up to 3065 K. Results of calculation of $\gamma_a(r)$, T_{pa}, $\varphi_{pa}(r)$, $j_a(r)$ and $q_a(r)$ distributions for different thermal states of the anode are given in Figures 9–13. Here, parameter $\gamma_a = n_m/(n_g + n_m)$, where n_m, n_g are the summary concentrations of heavy particles (atoms and ions) of metal and shielding gas, characterizes metal vapour content in near-anode plasma; T_{pa} is the temperature of plasma on the outer boundary of anode layer, and the other quantities were defined earlier. Curves *1–3* in the mentioned figures correspond to the following T_{s0} values: 2700, 3000; 3065 K (evaporating anode), dashed curves show the respective dependencies for an arc with nonevaporating anode at T_s = 500 K.

As follows from Figure 9, maximum content of metal vapour in arc plasma is achieved on anode layer axis, increasing with T_{s0}. Here, the maximum value of the rate of vapour outflow from anode surface also increases at the specified temperature rise. So, for instance, at T_{s0} = 3000 K this rate can reach the value of more than 10 m/s. Such an intensive flow of relatively cold vapour, moving from anode surface into the arc column, causes local cooling down of near-anode plasma. This effect is manifested in that part of the anode layer, which is adjacent to the most heated zone of anode surface, and the stronger, the higher is the surface temperature in this zone (see Figure 10).

Despite the fact that increase of the concentration of easily ionizable (compared to Ar) metal (Fe) vapour in near-anode plasma with T_{s0} rise should lead to increase of its electric conductivity σ, and, consequently, increase of electric current density, the above-noted effect of local cooling of plasma has a more essential role, causing a lowering of electric current density in paraxial zone of the region of anode

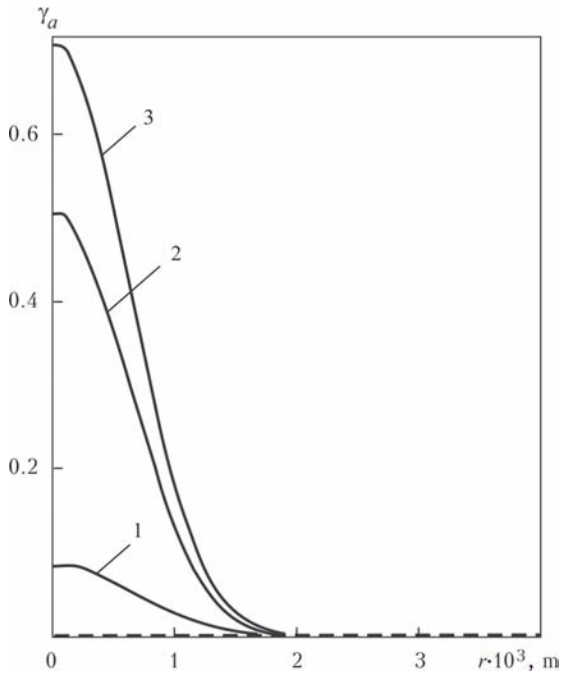

Figure 9. Radial distributions of the fraction of heavy particles of iron in multicomponent arc plasma (Ar–Fe) on the boundary of arc column with anode layer under the conditions characteristic for TIG welding of low-carbon steel in argon (for designations of curves *1–3* see the text)

attachment of the arc with evaporating anode, as follows from Figure 11.

The cause of such behaviour of value $j_a(r)$ in the case of evaporating anode is the shown in Figure 12 local decrease of plasma potential φ_{pa} in the center of the region of anode attachment of the arc, associated, according to the data in Figure 7, *a*, with the respective lowering of the temperature of near-anode plasma electrons (see Figure 10). Calculated dependencies of $\varphi_{pa}(r)$ shown in Figure 12, reveal that in case

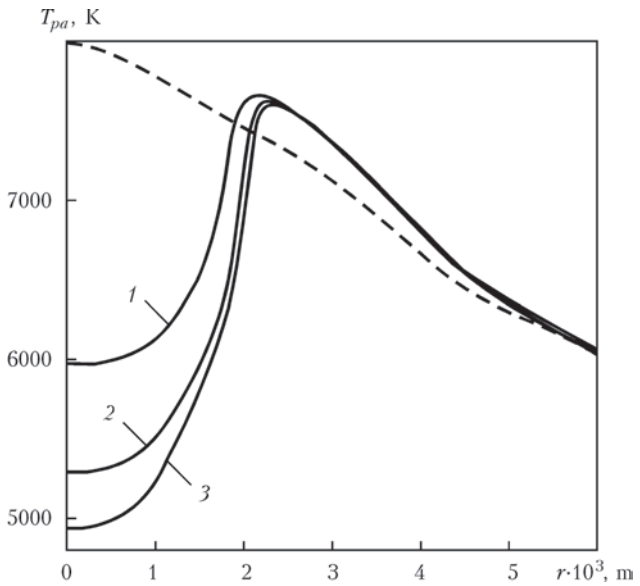

Figure 10. Radial distributions of arc column plasma temperature on the boundary with anode layer (for designations of curves *1–3* see the text)

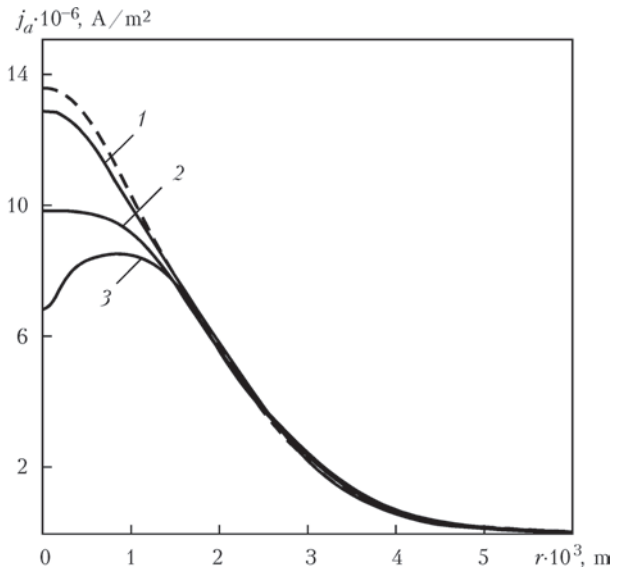

Figure 11. Radial distributions of anode current density (for designations of curves *1–3* see the text)

of evaporation of anode metal, a radial component of electric current density $j_{ar} = -\sigma_{pa}\frac{\partial\varphi_{pa}}{\partial r}$ appears on the boundary of anode layer with arc column, where σ_{pa} is the electric conductivity of plasma on the mentioned boundary. This component is directed towards the arc axis and increases with T_{s0} rise. It leads to an essential lowering of current density in the center of the region of anode attachment of the arc with evaporating anode relative to the arc with water-cooled (nonevaporating) anode.

Density of heat flow, contributed by the arc to the evaporating anode (see Figure 13) demonstrates similar behaviour. Considerable lowering of q_a at high temperatures of the anode surface, is related to reduction of the convective flow of energy from the arc column, as a result of the respective change of gas-dynamic

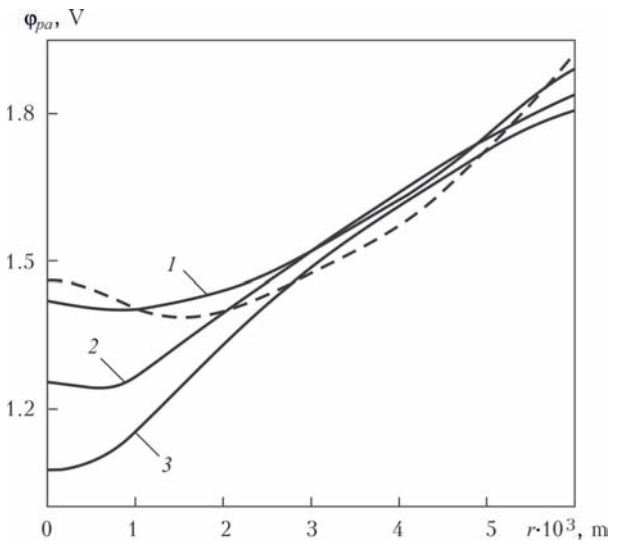

Figure 12. Radial distributions of arc plasma potential on the boundary of the anode layer with arc column (for designations of curves *1–3* see the text)

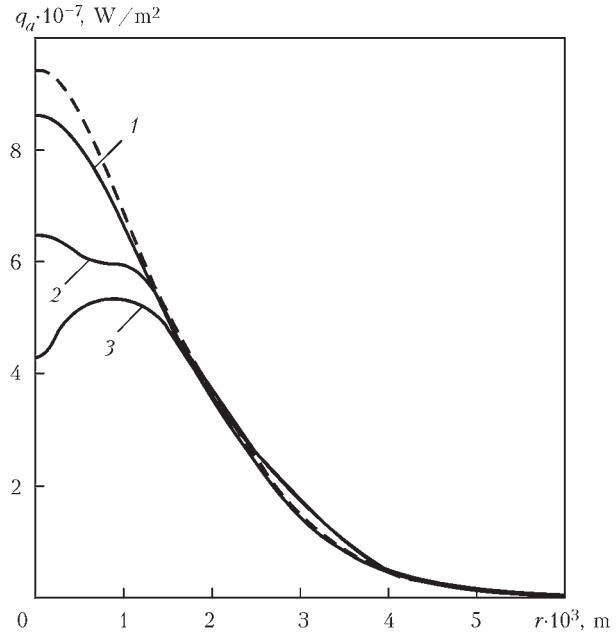

Figure 13. Radial distributions of heat flow applied by the arc to the anode (for designations of curves *1–3* see the text)

and electromagnetic situation in near-anode region of arc plasma, as well as to reduction of heat flow carried to the anode by electrons, owing to above-mentioned local reduction of j_a (see Figure 11).

We will perform qualitative analysis of the effect of nonuniformity of distribution of φ_{pa} or U_a values over the region of arc anode attachment and its impact on the features of welding arc burning, as well as on the nature of penetration of the metal being welded in TIG welding and electrode metal transfer in MIG/MAG welding.

Figure 14 schematically shows two possible distributions of electrical characteristics of arc plasma near the surface of metal being welded (anode), under the conditions, characteristic for spot TIG welding (weld pool is assumed to be axisymmetric, and its surface to be flat). Figure 14, *a* presents a situation, when distribution of electric potential on the boundary of anode layer with arc column $\varphi_{pa}(r)$ is an increasing function of radius (distance from arc axis). In this case, the radial component of current density on the above boundary $j_{ar} = -\sigma_{pa} \dfrac{\partial \varphi_{pa}}{\partial r}$ is negative, and accordingly, anode current density turns out to be smaller than that in arc column, and the transverse dimension of current channel is greater, that corresponds to a discharge distributed over the anode. In the opposite case, when $\partial\varphi_{pa}/\partial r < 0$ (see Figure 14, *b*) anode current density increases, and current channel radius becomes smaller, i.e. arc contraction on the anode $R_a^{(b)} < R_a^{(a)}$ is observed (see Figure 14, *a, b*). As a result, the electromagnetic force, applied to molten metal of the weld pool in its paraxial zone, turns out to be greater, than in the first case $F_{em}^{(b)} > F_{em}^{(a)}$ [31]. This leads to a more intensive convective heat transfer from the most heated central part of pool surface to its bottom, thus increasing the depth of penetration of the metal being welded (see Figure 14, *a, b*).

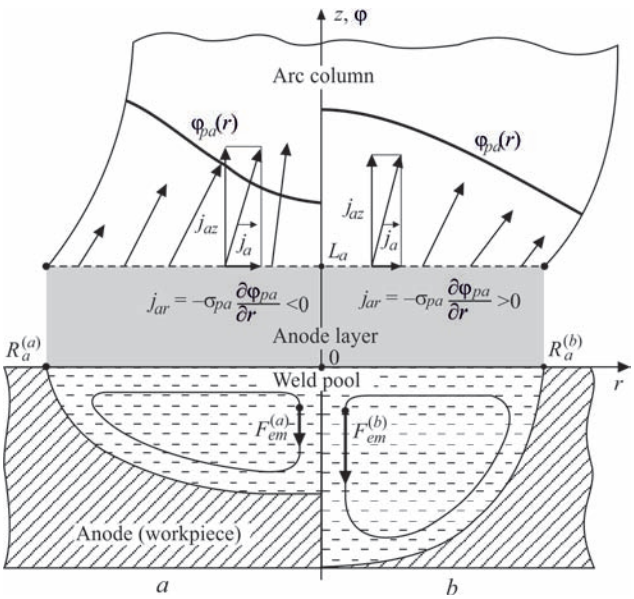

Figure 14. Schematic representation of electrical characteristics of near-anode plasma of the welding arc and process of metal penetration in TIG welding: *a* — discharge distributed over the anode surface; *b* — arc contraction on the anode

In the case of MIG/MAG welding, as shown in Figure 15, two variants of arc attachment to electrode metal drop are also possible. In the first case (see Figure 15, *a*), when distribution of electric potential on the boundary of anode layer with arc column $\varphi_{pa}(S)$ is the increasing function of coordinate *s*, measured from top of the drop along the generatrix of its surface, the tangential component of current density on the mentioned boundary $j_{as} = -\sigma_{pa} \dfrac{\partial \varphi_{pa}}{\partial s}$ is negative, and, accordingly, current density on the drop surface turns out to be smaller, than in the arc column, and area of arc anode attachment is larger than the cross-sectional area of its column, respectively. In the case, when $\partial\varphi_{pa}/\partial s < 0$ (see Figure 15, *b*), the tangential component of current density on the anode layer boundary is directed away from the drop top to arc periphery, that is manifested in arc contraction on the drop surface. As a result, $s_a^{(b)} < s_a^{(a)}$, and, accordingly, electromagnetic force applied to the drop turns out to be greater in the first case, than in the second case $F_{em}^{(a)} > F_{em}^{(b)}$ [32]. This leads to the drop size being smaller in the first case (see Figure 15, *a*) than in the second case (see Figure 15, *b*).

The above-noted nonuniformity of anode potential drop along the anode surface requires determination of integral (effective) value of anode drop $\langle U_a \rangle$, which summed up with appropriately determined

cathode potential drop $<U_c>$ and column voltage $<U_p>$ should, according to (1), yield total arc voltage $U = <U_c> + <U_p> + <U_a>$ As the potentials of the surface of metal anode and cathode can be considered constant with sufficient accuracy (because of the high electric conductivity of metal), arc voltage can be defined as the difference of potentials of the surface of anode and cathode, i.e. $U = \varphi_a - \varphi_c$ can be assumed (see Figure 1). However, such a generally accepted definition of voltage as an integral electrical characteristic of the arc discharge is not applicable for calculation of cathode and anode drops, as plasma potential on anode layer boundary φ_{pa}, as well as plasma potential on cathode layer boundary φ_{pc} are variable along boundaries Γ_{pa} and Γ_{pc}, separating the anode and cathode layers from the arc column.

We will introduce the concept of effective voltage drop as an integral electrical characteristic of current-conducting medium with nonisopotential boundaries [21]. As electric current density in arc column plasma is defined by expression $\vec{j} = -\sigma\nabla\varphi$, the following balance relationship follows from equation $\operatorname{div}\vec{j} = 0$:

$$\int_{\Omega}\frac{\left|\vec{j}\right|^2}{\sigma}dV = -\int_{\Gamma}\varphi j_n dS, \qquad (38)$$

where Ω is the region taken up by arc column plasma; Γ is its boundary; j_n is the projection of current density vector on outer normal $\vec{n}$ to Γ.

We will present boundary Γ in the following form: $\Gamma = \Gamma_{pa} + \Gamma_{pc} + \Gamma_{pe}$, where Γ_{pe} is the part of boundary Γ, through which the current does not flow ($j_n|_{\Gamma_{pe}} = 0$). Then, from (38) we obtain

$$\int_{\Omega}\frac{\left|\vec{j}\right|^2}{\sigma}dV = \int_{\Gamma_{pa}}\varphi_{pa} j_{an'} d\Gamma_{pa} - \int_{\Gamma_{pc}}\varphi_{pc} j_{cn} d\Gamma_{pc}, \qquad (39)$$

where $\vec{n}' = -\vec{n}$. The expression in the left-hand part of (39) is the thermal power released in the arc column. In keeping with integral Joule–Lenz law, we will write:

$$\int_{\Omega}\frac{\left|\vec{j}\right|^2}{\sigma}dV = I\left\langle U_p\right\rangle,$$

where by $<U_p>$ we will mean effective voltage drop in arc column,

$$\left\langle U_p\right\rangle = \frac{1}{I}\int_{\Omega}\frac{\left|\vec{j}\right|^2}{\sigma}dV.$$

As surfaces Γ_{pa} and Γ_{pc} are nonisopotential, we will introduce the concepts of effective values of potential Φ_{pa} and Φ_{pc} for them as follows:

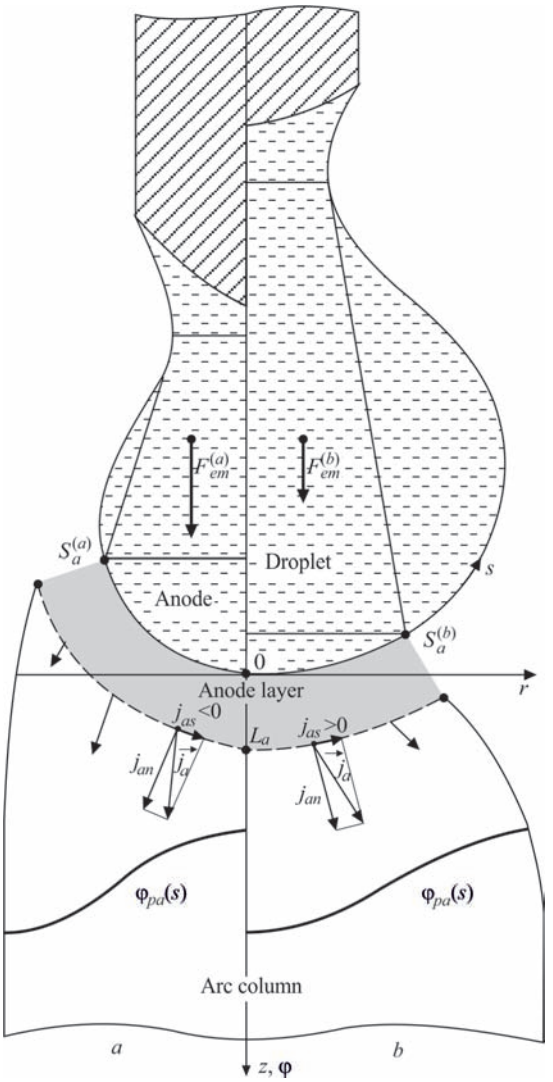

Figure 15. Schematic representation of electrical characteristics of near-anode plasma of the welding arc and process of electrode metal drop formation at MIG/MAG welding: *a* — discharge distributed over the anode surface; *b* — arc contraction on the anode

$$\Phi_{pa} = \frac{1}{I}\int_{\Gamma_{pa}}\varphi_{pa} j_{an'} d\Gamma_{pa};$$
$$\Phi_{pc} = \frac{1}{I}\int_{\Gamma_{pc}}\varphi_{pc} j_{cn} d\Gamma_{pc}. \qquad (40)$$

Then from (39) the voltage drop on arc column can be defined as the difference of effective values of potentials Φ_{pa} and Φ_{pc}, i.e. $<U_p> = \Phi_{pa} - \Phi_{pc}$ can be assumed. Using (40) we will define the effective anode $<U_a>$ and cathode $<U_c>$ drops in the following form: $<U_a> = \varphi_c - \Phi_{pa}$, $<U_c> = \Phi_{pc} - \varphi_c$. Within these definitions, we can obtain a standard expression for arc voltage in the form of the sum of voltage drops in separate portions of the arc discharge:

$$U = <U_c> + <U_p> + <U_a>, \qquad (41)$$

where one should bear in mind that the effective anode voltage drop is negative.

Finally, in terms of the thus introduced effective values of voltage drops the total power balance of arc discharge components can be written similar to (41):

$$P = <P_c> + <P_p> + <P_a>, \quad (42)$$

where $P = IU$, $<P_c> = I<U_c>$, $<P_p> = I<U_p>$, $<P_a> = I<U_a>$.

Note here that thermal power released in the arc column and cathode layer exceeds IU by value $|<P_a>|$, consumed for maintaining the anode layer.

1. Nemchinsky, V.A., Perets, L.N. (1977) Near-anode layer of high-current high-pressure arc. *ZhTF*, **47**, 1868–1875 [in Russian].
2. Dinulescu, H.A., Pfender, E. (1980) Analysis of the anode boundary layer of high intensity arcs. *J. of Appl. Phys*., **51**, 3149–315.
3. Dyuzhev, G.A., Nemchinsky, V.A., Shkolnik, S.M. et al. (1983) Anode processes in high-current arc discharge. *Khimiya Plazmy*, **10**, 169–209 [in Russian].
4. Nazarenko, I.P., Panevin, I.G. (1989) Analysis of the near-anode processes character in argon arc discharge of high pressure. *Contrib. Plasma Phys*., **29**, 251–261.
5. Nemchinsky, V.A. (1994) Size and shape of the liquid droplet at the molten tip of an arc electrode. *J. Phys. D: Appl. Phys.*, **27**, 1433–1442.
6. Jenista, J., Heberlein, J.V.R., Pfender, E. (1997) Numerical model of the anode region of high-current electric arcs. *IEEE Trans. on Plasma Sci.*, **25**, 883–890.
7. Amakawa, T., Jenista, J., Heberlein, J. et al. (1998) Anode-boundary-layer behavior in a transferred, high intensity arc. *J. Phys. D: Appl. Phys*., **31**, 2826–2834.
8. Tanaka, M., Ushio, M., Wu, C. S. (1999) One-dimensional analysis of the anode boundary layer in free-burning argon arcs. *Ibid.*, **32**, 605–611.
9. Murphy, A. B. (2010) The effects of metal vapour in arc welding. *Ibid*., **43**, 434001.
10. Zhu, P., Lowke, J.J., Morrow, R. et al. (1995) Prediction of anode temperatures of free burning arcs. *Ibid*., **28**, 1369–1376.
11. Lowke, J.J., Morrow, R., Haidar, J. (1997) A simplified unified theory of arcs and their electrodes. *Ibid.*, **30**, 2033–2042.
12. Fan, H.G., Kovacevic, R. (2004) A unified model of transport phenomena in gas metal arc welding including electrode, arc plasma and molten pool. *Ibid.*, **37**, 2531–2544.
13. Nishiyama, H., Sawada, T., Takana, H. et al. (2006) Computational simulation of arc melting process with complex interactions. *ISIJ Int.*, **46**, 705–711.
14. Hu, J., Tsai, H. L. (2007) Heat and mass transfer in gas metal arc welding. Pt 1: The arc. . *Int. J. Heat and Mass Transfer*, **50**, 833–846.
15. Masquere, M., Freton, P., Gonzalez, J.J. (2007) Theoretical study in two dimensions of the energy transfer between an electric arc and an anode material. *J. Phys. D: Appl. Phys*., **40**, 432–446.
16. Benilov, M.S. (2008) Understanding and modelling plasma-electrode interaction in high-pressure arc discharges (Review). *Ibid.*, **41**, 144001.
17. Lancaster, J.F. (1986) *The physics of welding*, 2nd Edition. Pergamon Press.
18. Sanders, N.A., Pfender, E. (1984) Measurement of anode falls and anode heat transfer in atmospheric pressure high intensity arcs. *J. of Appl. Phys*., **55**, 714–722.
19. Tanaka, M., Ushio, M. (1999) Observations of the anode boundary layer in free-burning arcs. *J. Phys. D: Appl. Phys*., **32**, 906–912.
20. Krivtsun, I., Demchenko, V., Lesnoi, A. et al. (2010) Modelling of electromagnetic processes in system «welding arc evaporating anode». Pt1: Model of anode region. *Sci. and Techn. of Welding and Joining*, **10**, 457–462.
21. Krivtsun, I., Demchenko, V., Krikent, I. et al. (2015) Distributed and integrated characteristics of the near-anode plasma of the welding arc in TIG and hybrid (TIG + CO_2-laser) welding. *Mathematical Modelling of Weld Phenomena 11 Techn. Universität Graz, Graz, Austria*, 837–874.
22. Semenov, I.L., Krivtsun, I. V., Reisgen, U. (2016) Numerical study of the anode boundary layer in atmospheric pressure arc discharges. *J. Phys. D: Appl. Phys*., **49**, 105204.
23. Almeida, N.A., Benilov, M.S., Naidis, G.V. (2008) Unified modelling of near-cathode plasma layers in high-pressure arc discharges. *Ibid.*, **41**, 245201.
24. Zhdanov, V.M. (2002) *Transport processes in multicomponent plasma*. London, Taylor&Francis.
25. Krivtsun, I.V. (2001) Model of evaporation of metal in arc, laser and laser-arc welding. *The Paton Welding J.*, **3**, 2–9.
26. Baksht, F.G., Dyuzhev, G.A., Mitrofanov, N.K. et al. (1973) Probe measurements in low-temperature dense plasma at high degree of ionization. *ZhTF*, 43(**12**), 2574–2583 [in Russian].
27. Chen, F. (1967) *Electrical probes*: Plasma disgnostics. Ed. by R. Huddleston et al. Moscow, Mir [in Russian].
28. Griem, H.R. (1962) High-density correction in plasma spectroscopy. *Phys. Rev*., **128**, 997–1001.
29. Krivtsun, I.V., Demchenko, V.F., Krikent, I.V. (2010) Model of the processes of heat, mass and charge transfer in the anode region and column of the welding arc with refractory cathode. *The Paton Welding J.*, **6**, 2–9.
30. Krikent, I.V., Krivtsun, I.V., Demchenko, V.F. (2014) Simulation of electric arc with refractory cathode and evaporating anode. *Ibid.*, **9**, 17–24.
31. Demchenko, V.F., Krivtsun, I.V., Krikent, I.V. et al. (2017) Force interaction of arc current with self magnetic field. *Ibid.*, **3**, 15–24.
32. Semenov, O., Demchenko, V., Krivtsun, I. et al. (2012) A dynamic model of droplet formation in GMA welding. *Modelling and Simulation in Materials Sci. and Engin.*, **20**, 045003.

Received 10.09.2018